Available online at www.sciencedirect.com
ScienceDirect
International Journal of Multiphase Flow 33 (2007) 873–896
International Journal of Multiphase Flow
www.elsevier.com/locate/ijmulflow

A new predictive model for fragmenting and non-fragmenting binary droplet collisions

Achuth Munnannur *, Rolf D. Reitz

Engine Research Center, 1500 Engineering Drive, University of Wisconsin-Madison, Madison, WI-53706, USA

Received 10 August 2006; received in revised form 6 March 2007

Abstract

A new predictive model for collisional interactions between liquid droplets, which is valid for moderate to high Weber numbers (>40), has been developed and validated. Four possible collision outcomes, viz., bouncing, coalescence, reflexive separation and stretching separation, are considered. Fragmentations in stretching and reflexive separations are modeled by assuming that the interacting droplets form an elongating ligament that either breaks up by capillary wave instability, or retracts to form a single satellite droplet. The outcome of a collision, number of satellites formed from separation processes and the post-collision characteristics such as velocity and drop-size are compared with available experimental data. The comparisons include colliding mono- and poly-disperse streams of droplets of different fuels under atmospheric conditions, and the results agree reasonably well.

Keywords: Drop collisions; Breakup; Coalescence; Capillary waves

1. Introduction

Reliable prediction of the outcome of a droplet collision is important in spray applications since it intimately affects the drop distribution (Gavaises et al., 1996) and therefore mixing and subsequent processes such as evaporation and combustion and pollutant formation in reactive systems. Experimental studies with low viscosity liquids that are useful in meteorological and energy applications have shown that at least the following three independent variables are of interest in characterizing a binary drop collision process:

(i) Drop Weber number (We), which is the ratio of the inertia force to the surface tension force, defined as $\rho U^2 d_s/\sigma$, where ρ is the liquid density, σ is the liquid surface tension, d_s is the diameter of the smaller drop and U is the relative velocity between the colliding drops.

* Corresponding author. Tel.: +1 608 265 8608; fax: +1 608 262 6707.
E-mail address: amunnannur@wisc.edu (A. Munnannur).

0301-9322/$ - see front matter © 2007 Elsevier Ltd. All rights reserved.
doi:10.1016/j.ijmultiphaseflow.2007.03.003

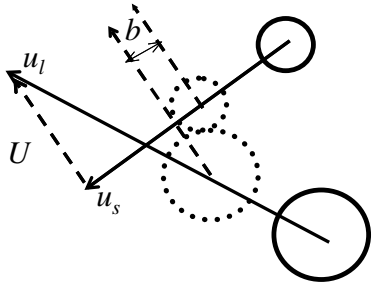

Fig. 1. Definition of the impact parameter in a binary droplet collision.

(ii) Impact parameter (b (dimensional) or B (non-dimensional)), which defines the geometrical orientation of the interacting drops. B is obtained by dividing the orthogonal distance b defined in Fig. 1 by the sum of the drop radii.
(iii) Drop-size ratio (Δ), which is the ratio of the size of the smaller drop to that of the larger drop.

The distinct outcomes of binary droplet interactions can be delineated on a Weber number–Impact parameter (We–B) plot for many test liquids of practical interest (Brazier-Smith et al., 1972; Ashgriz and Poo, 1990; Qian and Law, 1997), as shown in Fig. 2. However, the details of the We–B plot are dependent on the test liquid, background gas conditions and many other factors, such as the presence of fuel vapor in the ambience or cleanliness of liquid surfaces (Orme, 1997). The effects of thermal and surface tension gradients can also be critical in deciding the outcome of a collision (Neitzel and Dell'Aversana, 2002). Detailed modeling of free surface flows and boundary tracking methods have been used for drop collision modeling, but with large computational expenditure. The aim of the present work is to develop a model for practical sprays without substantial additional computational expense. Further, the emphasis is on the prediction of post-collision characteristics, as opposed to the prediction of the probability of collision, which merits considerable research in its own right (Schmidt and Rutland, 2000).

Interest in the physics of binary droplet collisions arose mainly from meteorological applications and hence most of the initial studies focused on colliding water droplets. Ashgriz and Poo (1990) reported experimental investigations and analytical results that have been used in developing physical collision models. Interest in the collision behavior of hydrocarbon fuel droplets is due to its relevance in spray combustion applications. Table 1 provides a summary of available experimental data with hydrocarbon fuels.

A priori prediction of the outcome of a collision can be made if We, B and Δ are known, and Table 2 provides a summary of approaches used for regime boundary predictions.

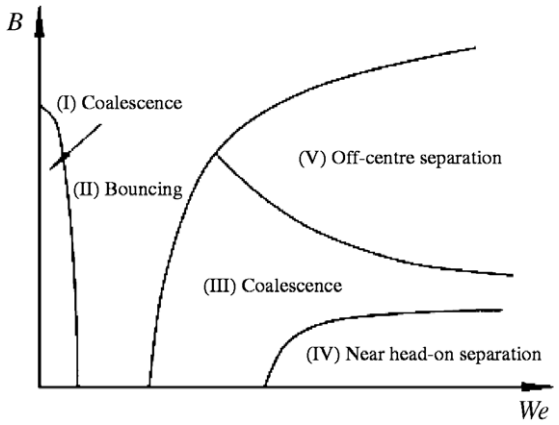

Fig. 2. Schematic of various collision regimes of hydrocarbon droplets in 1 atm. air (Qian and Law, 1997).

Table 1
Summary of experimental works on hydrocarbon droplet collisions

Authors	Test liquid	Weber numbers	Drop-sizes (μm)	Drop-size ratios	Ambient medium
Jiang et al. (1992)	Water, *n*-alkanes	Up to 100	150 (approx.)	1	Air
Qian and Law (1997)	Tetradecane, water	0.2–80	200–400	1	Nitrogen
Hung (1998)	Mineral spirits, diesel fuel	50–400 (approx.)	50–250 (approx.)	0.2–1 (approx.)	Air
Estrade et al. (1999)	Ethanol	Up to 220	80–300	1, 0.5	Air
Brenn et al. (2001)	Propanol-2	47–350	68–123	1	Air
Willis and Orme (2003)	Oils of different viscosities	203–4661	451–516	1	Vacuum

In the classical stochastic collision model of O'Rourke (1981), the efficiency of coalescence is estimated as

$$e_{\text{coal}} = \min\{1.0, [2.4f(\gamma)/We]\}, \tag{1}$$

where $f(\gamma) = \gamma^3 - 2.4\gamma^2 + 2.7\gamma$ and $\gamma = \frac{1}{\Delta}$. This expression was derived by assuming that the rotational energy of the combined mass formed by colliding drops should be less than the surface energy required to reform the drops, for coalescence to be permanent (Brazier-Smith et al., 1972). The impact parameter B is chosen as the square root of a uniform random number between 0 and 1. If $B > \sqrt{e_{\text{coal}}}$, the outcome of the collision is assumed to be a 'grazing' collision and the velocities of the interacting drops are specified from energy and momentum conservation. If u denotes the drop velocity, r the drop radius, and the subscripts i and j refer to the two interacting drops, the new drop velocities u_n are

$$u_{n,i} = \frac{r_i^3 u_i + r_j^3 u_j + r_j^3 (u_i - u_j) z}{r_i^3 + r_j^3}, \tag{2}$$

where $z = \left(\frac{B - \sqrt{e_{\text{coal}}}}{1 - \sqrt{e_{\text{coal}}}}\right)$ for grazing collisions.

If $B \leqslant \sqrt{e_{\text{coal}}}$, the outcome is assumed to be coalescence and the coalesced drop radius r_n and velocity u_n are given by

$$r_n = (r_i^3 + r_j^3)^{1/3} \tag{3}$$

and

$$u_n = \frac{r_i^3 u_i + r_j^3 u_j}{r_i^3 + r_j^3}. \tag{4}$$

In reality there are other outcomes from a binary droplet collision process, as shown in Fig. 2. Also, the O'Rourke model does not account for fragmentation and satellite drop formation in a non-coalescence collision.

Tennison et al. (1998) considered reflexive separation as an additional outcome. If the effective reflexive kinetic energy is more than 75% of the nominal surface energy of the combined spherical mass, reflexive separation is assumed to occur (Ashgriz and Poo, 1990). The Weber number criterion is

$$We > \frac{3[7(1+\Delta^3)^{2/3} - 4(1+\Delta^2)]\Delta(1+\Delta^3)^2}{(\Delta^6\eta_1 + \eta_2)}, \tag{5}$$

where $\eta_1 = 2(1-\xi)^2(1-\xi^2)^{1/2} - 1, \eta_2 = 2(\Delta - \xi)^2(\Delta^2 - \xi^2)^{1/2} - \Delta^3$ and $\xi = 0.5B(1+\Delta)$. Tennison et al. (1998) also did not account for the fragmentation of drops in a reflexive separation process. If We_{rflx} is the critical Weber number for reflexive separation, the velocities of the interacting drops were modified using Eq. (2) but assuming

$$z = \sqrt{1 - \frac{We_{\text{rflx}}}{We}}. \tag{6}$$

Georjon and Reitz (1999) proposed a model for collisions with fragmentation of drops. Drops that undergo grazing collisions were assumed to combine to form a uniform cylindrical liquid ligament whose temporal evolution is governed by a non-linear second order differential equation derived from mass and energy

Table 2
Regime boundary predictions in binary droplet collision modeling

Author(s)	Bouncing	Coalescence	Reflexive separation	Stretching separation	Shattering collisions
O'Rourke (1981)	Not considered	Coalescence efficiency from Brazier-Smith et al. (1972)	Not considered	From Brazier-Smith et al. (1972), any non-coalescence process	Not considered
Tennison et al. (1998)	Not considered	Brazier-Smith et al. (1972)	Criterion by Ashgriz and Poo (1990)	Brazier-Smith et al. (1972)	Not considered
Georjon and Reitz (1999)	Not considered	Brazier-Smith et al. (1972)	Not considered	Brazier-Smith et al. (1972)	If grazing collision, time-track the ligament
Estrade et al. (1999)	Correlation developed by Estrade et al. (1999)	Brazier-Smith et al. (1972)	Criterion by Ashgriz and Poo (1990) with added viscosity correction by Qian and Law (1997)	Brazier-Smith et al. (1972)	Not considered
Post and Abraham (2002)	Estrade et al. (1999)	Brazier-Smith et al. (1972)	Ashgriz and Poo (1990)	Brazier-Smith et al. (1972)	If reflexive separation and Weber number is above a threshold (100/1000)
Kollár et al. (2005)	Estrade et al. (1999)	Brazier-Smith et al. (1972)	Ashgriz and Poo (1990)	Brazier-Smith et al. (1972)	Not considered

conservation. Rayleigh's linear jet breakup theory was used to characterize satellite drops formed from the breakup of the ligament. Comparisons of predicted post-collision velocities and drop-sizes with the experimental results of Hung (1998) showed good qualitative agreement.

A 'composite' collision model was proposed by Post and Abraham (2002) that accounts for most of the outcomes in a wide range of Weber numbers, including bounce, reflexive separation, stretching separation, coalescence and shattering. To reduce the computational time, they proposed an approximate solution to the governing equation of the stretching ligament of Georjon and Reitz (1999) valid for high Weber numbers. However, they did not account for fragmentation in the reflexive and stretching separation processes. Dependency of the stretching separation process on impact parameter was also not considered.

Estrade et al. (1999) provided comprehensive information about the number of satellite drops formed from the collisions. They derived a criterion for drop bouncing by prescribing that the initial kinetic energy of the drop should not exceed the energy required to produce a limiting deformation, viz.,

$$We < \frac{\Delta(1+\Delta^2)(4\Theta' - 12)}{\chi_1\left\{\cos[\sin^{-1}(B)]\right\}^2}, \tag{7}$$

where Θ' a shape is factor of value 3.351 and χ_1 is a function of drop-sizes and impact parameter, where, for $0.5(d_s + d_l)(1 - B) > 0.5d_l$,

$$\chi_1 = 1 - 0.25(2-\tau)^2(1+\tau), \tag{8}$$

or, if $0.5\ (d_s + d_l)(1 - B) \leqslant 0.5d_l$,

$$\chi_1 = 0.25\tau^2(3-\tau). \tag{9}$$

Here $\tau = (1 - B)(1 + \Delta)$ and d_s and d_l are the diameters of the small and large drops, respectively.

Brenn et al. (2001) reported experiments with mono-disperse drops undergoing coalescence, reflexive separation or stretching separation and outlined stability nomograms to demarcate zones of constant number of satellite drops. They also proposed models for head-on and off-center collisions at high impact parameters, and compared predictions of the number of satellite drops with experimental observations of Ashgriz and Poo (1990) with reasonable agreement.

Kollár et al. (2005) proposed a composite collision model to simulate reflexive separation, stable coalescence and stretching separation. The model did not account for fragmentation in droplet collisions. Ko and Ryou (2005) proposed models for reflexive and stretching separation processes allowing for fragmentation of the volume separated from the colliding drops. The separating liquid volume from colliding drops was assumed to be proportional to both the net energy required for separation and the volume of the interaction region. This is a reasonable assumption because experimental images (Ashgriz and Poo, 1990; Qian and Law, 1997) show that only a portion of the interaction volume goes on to form satellite drops while the rest returns to the parent drops. Comparisons of the predicted number of satellite drops with available experimental data (Ashgriz and Poo, 1990; Brenn et al., 2001) showed some agreement. However, a physical mechanism for the breakup was not proposed.

In summary, in spite of the extensive literature, existing droplet collision models lack comprehensiveness and have not been adequately validated. It is important to establish confidence in the prediction of the outcome of a droplet collision process under controlled and deterministic conditions before extending the model to a spray. The primary objective of the present work was to develop a comprehensive, yet computationally inexpensive droplet collision model for determining the post-collision velocities and drop-sizes in binary drop collisions that occur under moderate to high Weber numbers (above 40). The approach followed is to decide the outcome of a collision from a *We–B* plot, and then determine the post-collision characteristics based on appropriate physical mechanisms. Sections 2 and 3 describe the details of the collision model, while Section 4 describes validation using deterministic collision models with comparisons to experimental data from the literature. Finally, in Section 5, conclusions are given and the validity and limitations of the model are discussed.

2. Collision model

The criterion for occurrence of various collision outcomes and a unified model for the prediction of post-collision drop characteristics are described in this section. The impact parameter is found deterministically from the orientation of the colliding drops.

2.1. Bouncing

In bouncing (region II in Fig. 2), droplets do not actually contact each other due to the layer of gas trapped in between them. When the impact parameter is low, bouncing takes place at lower Weber numbers. The probability for bouncing is increased at elevated ambient pressures (Qian and Law, 1997). The present study uses the criterion derived by Estrade et al. (1999) (Eqs. (7)–(9)) to determine the occurrence of bouncing. The post-collision velocities of the interacting drops are given by momentum and energy conservation, assuming no dissipation effects (viz., Eq. (2) with $z = 1.0$).

2.2. Coalescence

The droplets form a combined mass (temporary coalescence) that oscillates and remains a single entity (permanent coalescence – region III, Fig. 2). The Weber numbers are higher than those required for bouncing, so that the kinetic energy of the drops can expel the intervening gas film. The efficiency of coalescence is estimated with Eq. (1) and the post-collision characteristics are modeled with Eqs. (3) and (4).

2.3. Stretching separation

Droplets which collide at moderate to high impact parameters temporarily form a combined mass, but finally separate into two or more drops (region V, Fig. 2). The portion of the fluid in the droplet that does not experience contact continues to move in its original direction and the kinetic energy of this portion competes with the surface energy of the interaction region leading to eventual separation (e.g., Fig. 3). The criterion of Eq. (1) for predicting the incipience of stretching separation has been found to agree with available experimental data and is used in the present model.

The present model considers the temporal evolution of a ligament that is composed of part of the interacting volumes of the two drops. The major assumptions made in the model are:

(i) At the beginning of the stretching separation, drops form a uniform liquid ligament with bulbous end-drops. At the instant of separation, the radius of the cylindrical ligament is much less than the radius of the bulbous end-drops, consistent with experiments as in Fig. 3.
(ii) There is no rotation of drops immediately prior to or subsequent to the collision process.
(iii) The volume of the ligament remains constant throughout the stretching separation process. This assumes no drainage of mass from the smaller to the larger drop which is justified since the drainage effect is opposed by the stretching effect (Ashgriz and Poo, 1990).
(iv) If the net stretching energy is insufficient to overcome the sum of surface energy and viscous dissipation, no satellite droplet is formed. In this case the interacting drops simply undergo velocity changes as in Eq. (2).
(v) In stretching separation with fragmentation, the bulbous end-drops retain their original velocities but their sizes change to conserve mass. The velocities of the satellite drops formed from the ligament are determined from momentum and energy conservation.
(vi) The satellite drops formed from the fragmentation have equal sizes and velocities.

Ko and Ryou (2005) assumed that the ligament volume is equal to the product of the interaction volume of the drops and a separation volume coefficient (C_{vs}), calculated as the ratio of the energy required for separation to the total initial energy of the two droplets. They assumed that only the surface energy in the interaction area opposes the stretching kinetic energy. However, viscous dissipation in the interaction area offers

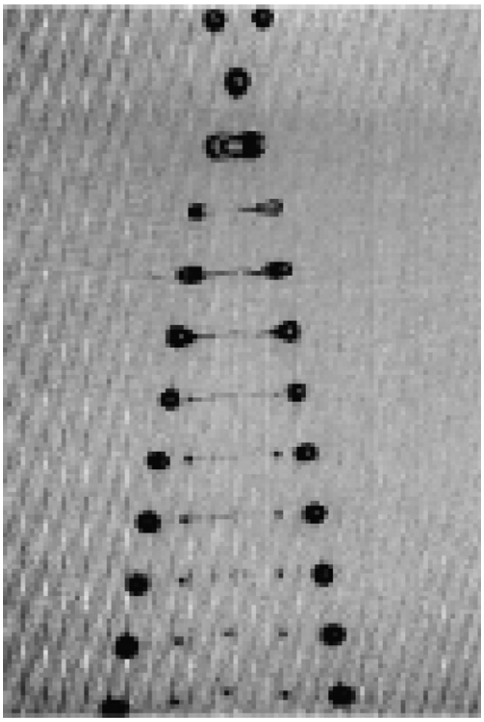

Fig. 3. Typical three satellite-drop stretching separation in colliding propanol-2 droplets (Brenn et al., 2001). Drop streams enter from top.

significant resistance to stretching when contact between the colliding drops is intense, which happens at intermediate impact parameters. Hence, the present collision model calculates a separation volume coefficient as

$$C_{\mathrm{vs}} = \frac{E_{\mathrm{strtch}} - E_{\mathrm{surten}} - E_{\mathrm{dissip}}}{E_{\mathrm{strtch}} + E_{\mathrm{surten}} + E_{\mathrm{dissip}}}, \tag{10}$$

where E_{strtch} is the total effective stretching kinetic energy, E_{surten} is the surface energy in the region of interaction and E_{dissip} is the viscous dissipation in the interaction region. The fraction of the volume lost from the smaller drop to form the ligament during collision is estimated as

$$\psi_{\mathrm{s}} = C_{\mathrm{vs}}\varphi_{\mathrm{s}}, \tag{11}$$

where, if $0.5(d_{\mathrm{s}} + d_{\mathrm{l}})(1 - B) > 0.5d_{\mathrm{s}}$,

$$\varphi_{\mathrm{s}} = 1 - \frac{(2\Delta - \tau)^2(\Delta + \tau)}{4\Delta^3}, \tag{12}$$

or, if $0.5(d_{\mathrm{s}} + d_{\mathrm{l}})(1 - B) \leqslant 0.5d_{\mathrm{s}}$,

$$\varphi_{\mathrm{s}} = \frac{\tau^2(3\Delta - \tau)}{4\Delta^3}, \tag{13}$$

where $\tau = (1 - B)(1 + \Delta)$. The fraction of the volume lost from the larger drop to form the ligament during the collision is estimated as

$$\psi_{\mathrm{l}} = C_{\mathrm{vs}}\varphi_{\mathrm{l}}, \tag{14}$$

where, if $0.5(d_{\mathrm{s}} + d_{\mathrm{l}})(1 - B) > 0.5d_{\mathrm{l}}$,

$$\varphi_{\mathrm{l}} = 1 - \frac{(2 - \tau)^2(1 + \tau)}{4\Delta^3}, \tag{15}$$

or, if $0.5(d_s + d_l)(1 - B) \leqslant 0.5d_l$,

$$\varphi_l = \frac{\tau^2(3-\tau)}{4}. \tag{16}$$

To estimate C_{vs}, the energies E_{strtch} and E_{surten} are (Ashgriz and Poo, 1990)

$$E_{strtch} = \frac{1}{2}\rho U^2 \left(\frac{1}{6}\pi d_l^3\right)\left(\frac{\Delta^3}{(1+\Delta^3)^2}\right)\left[(1+\Delta^3) - (1-B^2)(\varphi_s + \Delta^3\varphi_l)\right], \tag{17}$$

$$E_{surten} = \sigma\left[2\pi\left(\frac{1}{6}\pi d_l^3\right) d_l \tau(\Delta^3\varphi_s + \varphi_l)\right]^{1/2}. \tag{18}$$

Jiang et al. (1992) conducted experiments that showed that the energy dissipation associated with significant drop distortion, which precedes small amplitude free oscillations of the droplet, is independent of the liquid viscosity. However, Willis and Orme (2003), from experiments with colliding viscous oil drops in vacuum, concluded that the energy dissipation actually increases with viscosity. The present collision model follows Jiang et al.'s (1992) approach to estimate E_{dissip} in the interaction region because it allows a simple, *a priori* estimation of viscous dissipation and has been validated for hydrocarbon fuels. The model assumes E_{dissip} to be 30% of the total initial kinetic energy of the droplets for a stretching separation process, since this estimate was found to give reasonable predictions of the onset of satellite formation and number of satellites formed, as will be shown later in Section 4.2.

Mass conservation for an inviscid fluid ligament, neglecting the volumes of the rounded ends gives

$$\frac{4}{3}\pi r_s^3 + \frac{4}{3}\pi r_l^3 = (1-\psi_s)\frac{4}{3}\pi r_s^3 + (1-\psi_l)\frac{4}{3}\pi r_l^3 + \pi r^2\delta, \tag{19}$$

where r is the instantaneous radius of the ligament, δ is its instantaneous length, r_s is the radius of the smaller drop before collision, r_l is the radius of the larger drop before collision. Assuming no heat or work transfers, energy conservation gives

$$\begin{aligned}
&\rho\left(\frac{1}{2}\cdot\frac{4}{3}\pi r_s^3\cdot u_s^2 + \frac{1}{2}\cdot\frac{4}{3}\pi r_l^3\cdot u_l^2\right) + 4\pi r_s^2\sigma + 4\pi r_l^2\sigma \\
&\quad = \rho\left(\frac{1}{2}\cdot(1-\psi_s)\cdot\frac{4}{3}\pi r_s^3\cdot u_s^2 + \frac{1}{2}\cdot(1-\psi_l)\cdot\frac{4}{3}\pi r_l^3\cdot u_l^2\right) + \rho\cdot\left(\frac{1}{2}\pi r^2\delta V_r^2\right) \\
&\qquad + 2\pi\sigma r_{bs}\left(r_{bs} + \sqrt{(r_{bs}^2 - r^2)}\right) + 2\pi\sigma r_{bl}\left(r_{bl} + \sqrt{(r_{bl}^2 - r^2)}\right) + \sigma(2\pi r\delta) + \Phi,
\end{aligned} \tag{20}$$

where u_s is the velocity of the small drop, u_l is the velocity of the large drop, r_{bs} is the radius of the smaller drop after collision, r_{bl} is the radius of the larger drop after collision, V_r is the average velocity of the fluid inside the ligament and Φ is the viscous dissipation. The governing equation for the ligament evolution is derived by differentiating Eq. (20) with respect to time. By virtue of the model assumptions, u_s and u_l are independent of time. Further, $\delta \gg r$, $r_{bs} \gg r$ and $r_{bl} \gg r$. Using these simplifications in Eq. (20) and differentiating it with respect to time, one can obtain

$$\left((\pi r^2\delta)(V_r^2)\right)' + \left(\frac{4\pi\sigma}{\rho}\right)(r\delta)' + \left(\frac{2\Phi'}{\rho}\right) = 0, \tag{21}$$

where prime denotes derivative with respect to time. Since the ligament volume $\pi r^2\delta$ is assumed to be independent of time, Eq. (21) can again be simplified to

$$(V_r^2)' - \left(\frac{4\sigma r'}{\rho r^2}\right) + \left(\frac{2\Phi'}{\rho\pi r^2\delta}\right) = 0. \tag{22}$$

The initial shape of the mass that connects the bulbous end-drops is assumed to be a uniform cylinder of length equal to its radius. Then

$$r^2\delta = r_0^3, \tag{23}$$

where r_0 is the initial radius of the ligament given by

$$r_0 = \left[\left(\frac{4}{3}\right)(\psi_s r_s^3 + \psi_1 r_1^3)\right]^{1/3}. \tag{24}$$

The average fluid velocity in the stretching ligament is assumed to be proportional to the rate of stretching so that

$$V_r = A\delta', \tag{25}$$

where A is a constant assumed to be unity (Georjon and Reitz, 1999). The viscous dissipation is given by

$$\Phi = \mu \int\int \frac{1}{2}\left(\frac{\partial v_i}{\partial x_j} + \frac{\partial v_j}{\partial x_i}\right)^2 \mathrm{d}t\,\mathrm{d}x^3, \tag{26}$$

where μ is the liquid viscosity. For pure extensional flow, since $\dfrac{\partial V_r}{\partial z} \sim \dfrac{\delta'}{\delta}$,

$$\Phi' = \frac{\pi r^2 \mu \delta'^2}{2\delta}. \tag{27}$$

Using Eqs. (23), (25) and (27) in Eq. (22), the complete equation with viscous effects included can be obtained as

$$r'' = \left(\frac{3r'^2}{r}\right) + \left(\frac{\sigma r^4}{2\rho r_0^6}\right) - \left(\frac{\mu r^4 r'}{2\rho r_0^6}\right). \tag{28}$$

Choosing the initial radius r_0 and the capillary break-up time $t_\sigma = (\rho r_0^3/\sigma)^{1/2}$ as scaling variables to form a non-dimensional radius $\bar{r} = r/r_0$ and non-dimensional time $\bar{t} = t/t_\sigma$, Eq. (28) becomes

$$\bar{r}'' = \left(\frac{3\bar{r}'^2}{\bar{r}}\right) + \frac{\bar{r}^4}{2} - \frac{Oh_0}{\sqrt{2}}\bar{r}^4\bar{r}', \tag{29}$$

with initial conditions, $\bar{r}_{(0)} = 1$ and $\bar{r}'_{(0)} = -3\alpha\sqrt{We_0}/8\sqrt{2}$, where $Oh_0 = \mu/\sqrt{\rho(2r_0)\sigma}$, $We_0 = \rho U^2(2r_0)/\sigma$ and α is a model constant that empirically accounts for the initial shape transformation of the mass that connects the bulbous end-drops. The ligament radius at break-up is of interest in order to calculate the satellite drop-size. For low viscosity liquids where the thinning of the ligament due to stretching is not opposed significantly by viscous forces, the term involving the Ohnesorge number is small. Also, terms with $\bar{r}^4$ can be dropped to recover the equation valid for high Weber numbers proposed by Post and Abraham (2002)

$$\bar{r}'' = \left(\frac{3\bar{r}'^2}{\bar{r}}\right), \tag{30}$$

whose solution is

$$r = \left(\frac{r_0}{\sqrt{1 + \frac{3}{4r_0}\alpha U t}}\right). \tag{31}$$

Interestingly, the solution is similar to that of a capillary jet with linearly varying axial velocity (Frankel and Weihs, 1985) or for a falling inviscid liquid ligament (Henderson et al., 2000). The present fluid ligament is of finite length with its diameter diminishing with time and hence the rate of growth of instability is not a constant. Stability analysis in such situations involves the computationally expensive temporal tracking of the most unstable wave number. At low Weber numbers, an end-pinching mechanism (Stone et al., 1986; Qian and Law, 1997) has been proposed to be responsible for ligament breakup, but capillary instability may be the dominant breakup mechanism at high elongations of the ligament (Stone, 1994). Willis and Orme

(2003) show that capillary instability is the mechanism of ligament breakup at high collision Weber numbers. Thus, capillary instability analysis for a round liquid jet is employed in the present study (Reitz and Bracco, 1986).

When Rayleigh-type instability is responsible for ligament breakup, the time for break-up t_{bu} is related to ligament radius at breakup r_{bu} by Reitz and Bracco (1986) and Georjon and Reitz (1999)

$$t_{bu} = \frac{k_1}{0.34}\sqrt{\frac{\rho}{\sigma}} r_{bu}^{3/2}, \tag{32}$$

where k_1 is a constant. The radius of drops formed from the fragmentation is

$$r_{child} = 1.89 r_{bu}. \tag{33}$$

Using Eqs. (31) and (32), the non-dimensional ligament radius at break-up $\bar{r}_{bu} = r_{bu}/r_0$ is

$$\left(\frac{0.75}{\sqrt{2}}\right)(k_1\alpha) We_0^{1/2} \bar{r}_{bu}^{7/2} + \bar{r}_{bu}^2 - 1 = 0, \tag{34}$$

where k_1 and α are assumed to be 8.5 and 0.44, respectively, to give favorable comparisons with experimental results (see Section 4.2).

An inadequacy of the approximate solution to the equation of the ligament, not seen with the time-tracked numerical solutions is that the retraction of the ligament and subsequent satellite drop formation cannot be predicted. An important time scale for low Weber numbers is

$$T = t_\sigma \frac{\delta}{\delta'}, \tag{35}$$

which is the ratio of the capillary time scale t_σ to the time scale of elongation of the fluid ligament. $T \ll 1$, is the slow extension limit with volume contraction, while if $T \gg 1$ the break-up occurs before any significant stretching (Frankel and Weihs, 1985; Marmottant and Villermaux, 2004). Brenn et al. (2001) observed that a single satellite droplet is the most probable outcome of separation for the range of Weber numbers in their experiments (47–350). Thus, the present study considers the formation of a single satellite drop as the only outcome of a contraction process and if T is less than or equal to 2, it is assumed that the ligament contracts to form a single satellite drop. Table 3 summarizes the procedure used to calculate number of satellites and the size of satellite drops in stretching separation.

Post and Abraham's (2002) approximate solution to Eq. (30) assumes the ligament volume to be independent of impact parameter, and hence that solution cannot be used in the present study. Instead an approximate iterative solution method was adopted to solve the non-linear algebraic equation Eq. (34) based on linearizations of the non-linear term $\bar{r}_{bu}^{7/2}$ and successive iterations of the solutions. By this method, the exact solution to the following linearized equation is first obtained:

$$\left(\frac{0.75}{\sqrt{2}}\right)(k_1\alpha) We_0^{1/2} \bar{r}_{bu}^{4} + \bar{r}_{bu}^2 - 1 = 0. \tag{36}$$

Then, this is used in solving another linearized equation

$$\left(\frac{0.75}{\sqrt{2}}\right)(k_1\alpha) We_0^{1/2} \bar{r}_{bu}^{3} + \bar{r}_{bu}^2 - 1 = 0. \tag{37}$$

Table 3
Details of modeling fragmentation in stretching separation

Criterion	Physical process	Radius of satellite drop(s)	Number of satellite drop(s)
$C_{vs} \leqslant 0$	Grazing collision without fragmentation (Eq. (2))	Not applicable	None
$C_{vs} > 0$ and $T \leqslant 2$	Ligament contraction into a single satellite	r_0 From Eq. (24)	1
$C_{vs} > 0$ and $T > 2$	Ligament stretching and capillary break-up	Eqs. (33) and (34)	From mass conservation of the ligament assuming satellites of uniform size

This process is repeated in an iterative fashion. Four iterations are found to give converged solution to the non-linear equation in various cases which were tested and this adds very little to the computational time. Fig. 4 compares the predicted non-dimensionalized ligament length at break-up with a fourth order Runge–Kutta solution for tetradecane droplets (diameter 100 μm and impact parameter 0.75) and adequate agreement is seen.

2.4. Reflexive separation

Droplets which collide at low impact parameters (near "head-on") undergo temporary coalescence, but finally separate into two or more drops (region IV, Fig. 2). The process is composed of an oblate phase, where the droplets form an outward spreading disk or torus, and a prolate phase during which an outward stretching ligament is formed which breaks-up to produce drops (see Fig. 5). The present study uses Eq. (5) to predict the occurrence of reflexive separation.

In reflexive separation, the number of drops formed from fragmentation does not appear to be as strong a function of impact parameter as in stretching separation (Estrade et al., 1999; Brenn et al., 2001) because due to the intense contact, significant droplet deformation occurs and complex flow fields are generated within the ligament. This also increases difficulty in proposing a simple model, as for stretching separation. For instance, Morozumi et al. (2005) found it difficult to formulate a criterion between permanent coalescence and separation for water droplets that collide head-on.

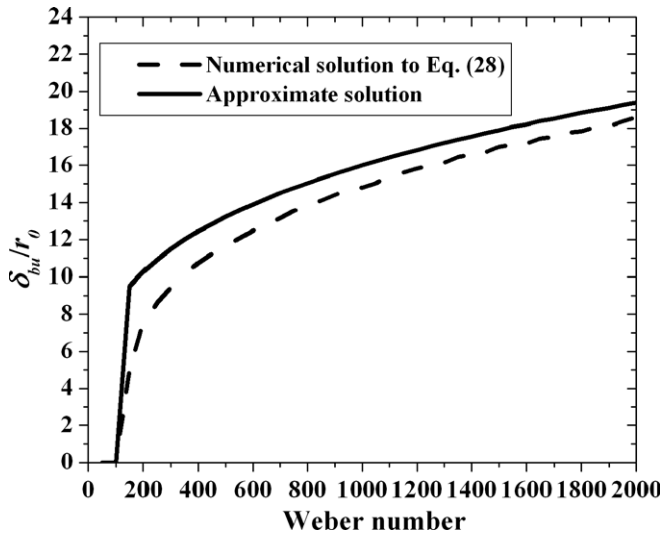

Fig. 4. Comparison of the non-dimensional ligament length at break-up as a function of Weber number as predicted by numerical solution and approximate iterative solution – tetradecane droplets of diameter 100 μm colliding at impact parameter of 0.75.

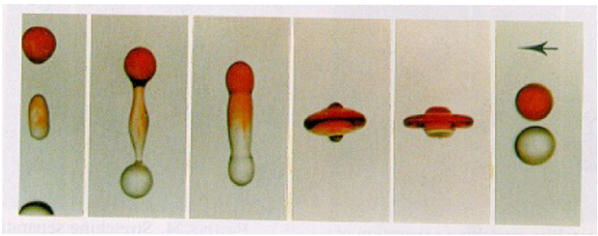

Fig. 5. Typical three-drop reflexive separation in colliding water droplets (Ashgriz and Poo, 1990). Drops enter from right.

The present model does not consider fragmentations that occur during the oblate phase (termed 'shattering' by Willis and Orme, 2003), because it requires very high initial kinetic energy and is considered to be only of secondary importance in the present study. Instead, reflexive separation is modeled from the incipience of the prolate phase by considering the temporal evolution of a stretching ligament. The major model assumptions are:

(i) At the incipience of the prolate phase, the colliding drops form a uniform cylindrical ligament with rounded ends. This is a reasonable approximation to the fourth image from the right in Fig. 5. The ligament volume is equal to the sum of the volumes of the interacting drops and is independent of the impact parameter.
(ii) The drops formed from the ligament break-up are uniform in size and velocity. Two of these form the end-drops while the remaining liquid will form satellite drops.
(iii) The velocities of the post-collision drops are calculated by momentum and energy conservation.
(iv) If T in Eq. (35) is less than or equal to 3, it is assumed that the ligament contracts to form a single child drop and two end-drops, all of the same size. The value 3 is chosen because it gave favorable comparisons with experimental data (see Section 4.3).

Assuming that the fluid velocity within the ligament is proportional to the rate of stretching and the initial shape to be a sphere, the governing equation for the ligament is

$$r'' = \left(\frac{9\sigma r^4}{32\rho r_0^6}\right) - \left(\frac{27\sigma r^7}{32\rho r_0^9}\right) + \left(\frac{3r'^2}{r}\right) - \left(\frac{9\mu r^4 r'}{32\rho r_0^6}\right), \tag{38}$$

where r_0 is the initial radius of the ligament given by

$$r_0 = (r_s^3 + r_1^3)^{1/3}. \tag{39}$$

For high Weber numbers, Eq. (38) can again be simplified to Eq. (30), and the approximate linearized solution can be found. Table 4 summarizes the procedure used to calculate number of satellites and the size of satellite drops in reflexive separation.

The ligament evolution occurs in the prolate phase of reflexive separation and the initial conditions should account for the energy dissipation that has occurred since drop contact. Fifty percentage of the total initial kinetic energy of the droplets was assumed to be dissipated at the incipience of the prolate phase, consistent with the experimental observations of Willis and Orme (2003) that the amplitude of deformation of the post-collision mass increases with increasing Weber numbers. The dissipated energy (E_{visc}) is subtracted from the total energy of the droplets before collision (E_0) (the sum of the kinetic and surface energies of the two drops) to estimate the velocity coefficient

$$C_v = \sqrt{1 - \frac{E_{visc}}{E_0}}. \tag{40}$$

This coefficient is multiplied by the original value $0.75\alpha U/2$ suggested by Georjon and Reitz (1999), to give the initial value of the average fluid velocity inside the ligament. α is chosen to be 0.45, as in stretching separation.

Table 4
Details of modeling fragmentation in reflexive separation

Criterion	Physical process	Radius of satellite drop(s)	Number of satellite drop(s)
$T \leqslant 3$	Ligament contraction into a single satellite	r_0 From Eq. (39)	1
$T > 3$	Ligament stretching and capillary break-up	Eqs. (33) and (34), but using r_0 From Eq. (39)	Total number of drops found from mass conservation of the ligament assuming drops of uniform size. Two of these are end-drops and the rest are satellites

3. Note on separation at high Weber numbers

From the regime plot of Fig. 2, it is seen that the region of coalescence becomes narrower as the Weber number increases, and the reflexive and stretching separation regimes may eventually overlap. Specifically, since the probability of stretching separation is calculated from the coalescence efficiency (Eq. (1)), there is a possibility for reflexive separation at high Weber numbers to be treated as stretching separation. To distinguish the processes, for any potential stretching separation process, the total stretching energy was estimated from Eq. (17) and the total reflexive energy was estimated as (Ashgriz and Poo, 1990)

$$E_{\mathrm{rflx}} = \sigma\pi d_1^2 \left[(1+\Delta^2) - (1+\Delta^3)^{2/3} + \frac{We(\Delta^6\eta_1 + \eta_2)}{12\Delta(1+\Delta^3)^2} \right]. \tag{41}$$

If the reflexive energy was higher than the stretching energy, the process is treated as a reflexive separation; otherwise, it is treated as a stretching separation.

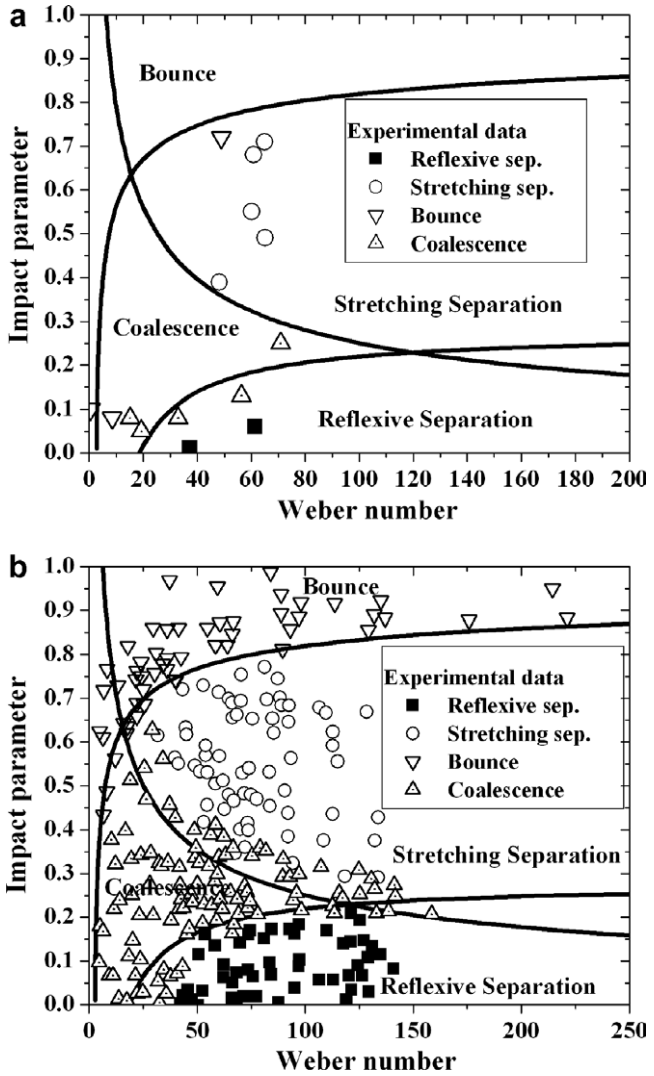

Fig. 6. Predicted regime boundaries for equal-size droplets (lines). (a) Experiments of Qian and Law (1997) for tetradecane droplets at atmospheric pressure. (b) Experiments of Estrade et al. (1999) for ethanol droplets at atmospheric pressure.

4. Model validation results

The present model was validated using available experimental data. First, the ability of the model to predict the regime boundaries of binary drop collisions is discussed. Validation of the stretching and reflexive separation models is then presented. Finally, the collision model was implemented into a CFD code and the results of the simulation are compared with available data for colliding streams of poly-disperse droplets.

4.1. Validation of collision regimes

Fig. 6a shows the predicted regime boundaries for binary droplet collisions between equally sized drops together with experimental results from Qian and Law (1997) for tetradecane droplets colliding at atmospheric

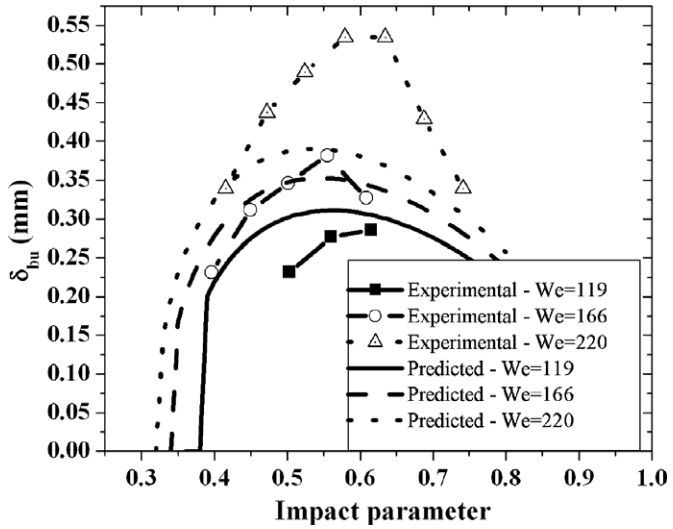

Fig. 7. Predicted ligament lengths at break-up at various Weber numbers compared to experimental results (Brenn et al., 2001) for colliding equal-size propanol-2 drops of 80 μm diameter.

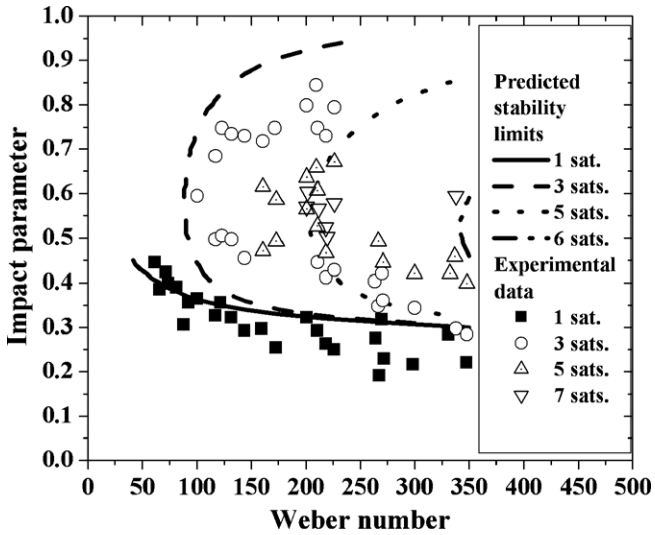

Fig. 8. Predicted boundaries for the formation of satellite drops in stretching separation for colliding equal-size propanol-2 drops of 110 μm diameter. Experimental results of Brenn et al. (2001) are shown.

pressure. Fig. 6b shows the predicted regime boundaries with experimental results from Estrade et al. (1999) for ethanol droplets at atmospheric pressure. It is seen that the agreement is quite reasonable for both test liquids.

4.2. Validation of stretching separation

The present model predictions were compared with experimental results of Brenn et al. (2001) to validate the stretching separation model. They report that two 89.3 μm propanol-2 drops colliding at a Weber number of 143 and impact parameter of 0.35, produced end-drops of diameter 86.7 μm and a satellite drop of diameter 37.9 μm. Under the same conditions, the present model predicts 88.6 μm and 31.5 μm as the diameters of the end-drops and the single satellite drop, respectively.

Fig. 7 compares measured and predicted lengths of the ligament at the instant of separation from the boundary drops as a function of impact parameter. Again, the comparisons show good qualitative agreement.

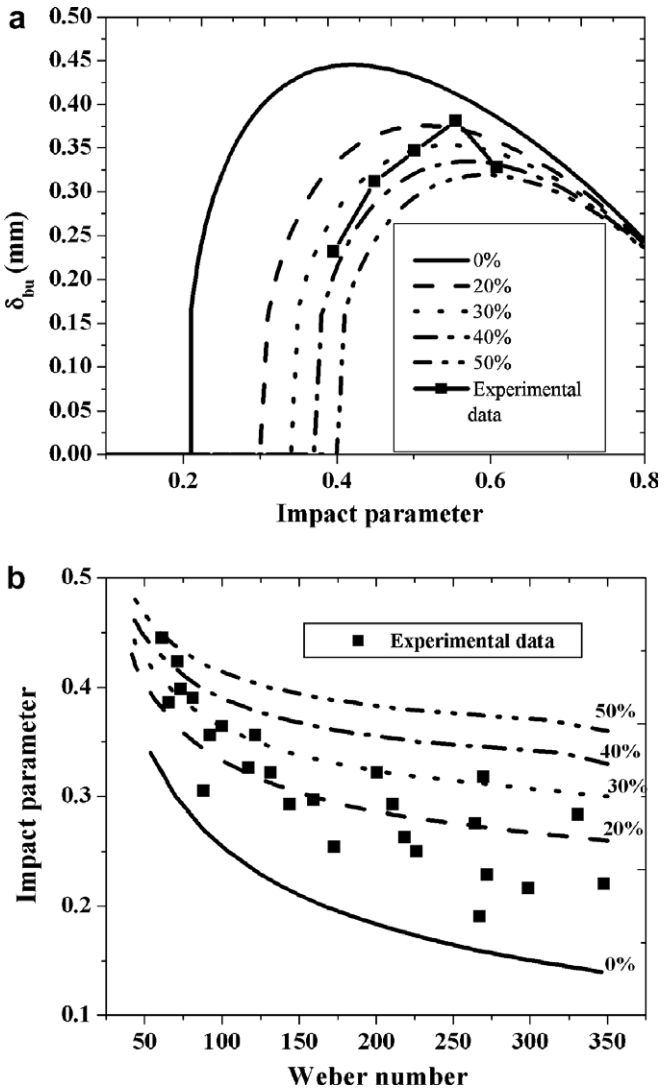

Fig. 9. Stretching separation predictions for various estimates of viscous energy dissipation (expressed as the percentage of total initial kinetic energy). (a) Ligament lengths at break-up for $We = 177$. All conditions same as in Fig. 7. (b) Boundaries for the formation of single satellite drop. All conditions same as in Fig. 8.

Brenn et al. (2001) also report the existence of specific zones in the *We–B* plane that exhibit a constant number of satellite droplets, as shown in Fig. 8. There is good agreement between the model predictions and the experimental results.

As mentioned in Section 2.3, it was assumed that the viscous energy dissipation in the interaction region in stretching separation is equal to 30% of the initial kinetic energy of the drops. This quantity appears in the separation volume coefficient (Eq. (10)) and decides not only the occurrence of fragmentation, but also the magnitude of the ligament volume and subsequently post-fragmentation characteristics (number of satellites, satellite drop-size). It is appropriate to assess the sensitivity of this estimate on the predictions. Fig. 9a shows the predicted ligament lengths obtained for different values of the amount of viscous energy dissipated for the $We = 166$ conditions of Fig. 7. As the dissipation is increased for the same Weber number, the onset of satellite formation occurs at higher impact parameters. The impact parameter at which the ligament length reaches a maximum also moves to the right. Fig. 9b compares the predicted stability limit for single satellite formation against experimental results (which was shown in Fig. 8) for different values of the amount of viscous energy dissipated. Comparisons for other numbers of satellite drops were also attempted. From the sensitivity analysis, it appears necessary to account for viscous dissipation in the interaction region to correctly capture the satellite formation process. From the tests, a value between 25% and 35% of the total initial kinetic energy appears to be reasonable for stretching separation.

Since binary droplet collision behavior is dependent on the liquid properties, it was of interest to compare results for different hydrocarbon fuels. Estrade et al. (1999) report the number of satellite droplets for various Weber numbers and impact parameters for ethanol droplets as shown in Fig. 10. The agreements are reasonable for up to three satellite drops, but the results are not as good for five or more satellites. In summary, the model predictions show the following qualitative trends which have also been observed experimentally:

(i) The number of satellite drops increases as the Weber number increases.
(ii) For a given Weber number, the number of satellite drops first increases with the impact parameter, reaches a maximum and then decreases.

4.3. Validation of reflexive separation

Fig. 11a shows the predicted variation of the number of satellite drops with Weber number, for colliding 110 μm diameter propanol-2 drops, while Fig. 11b shows predictions for 200 μm ethanol droplets. In Fig. 11a,

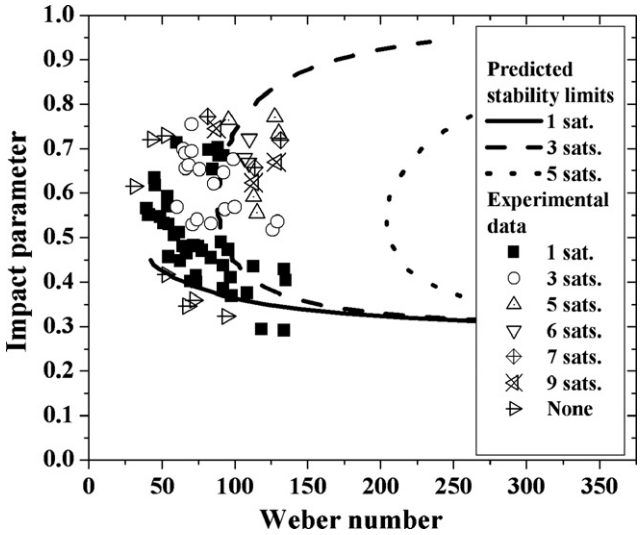

Fig. 10. Predicted boundaries for the formation of satellite drops in stretching separation for colliding equal-size ethanol drops of 200 μm diameter. Experimental results of Estrade et al. (1999) are shown.

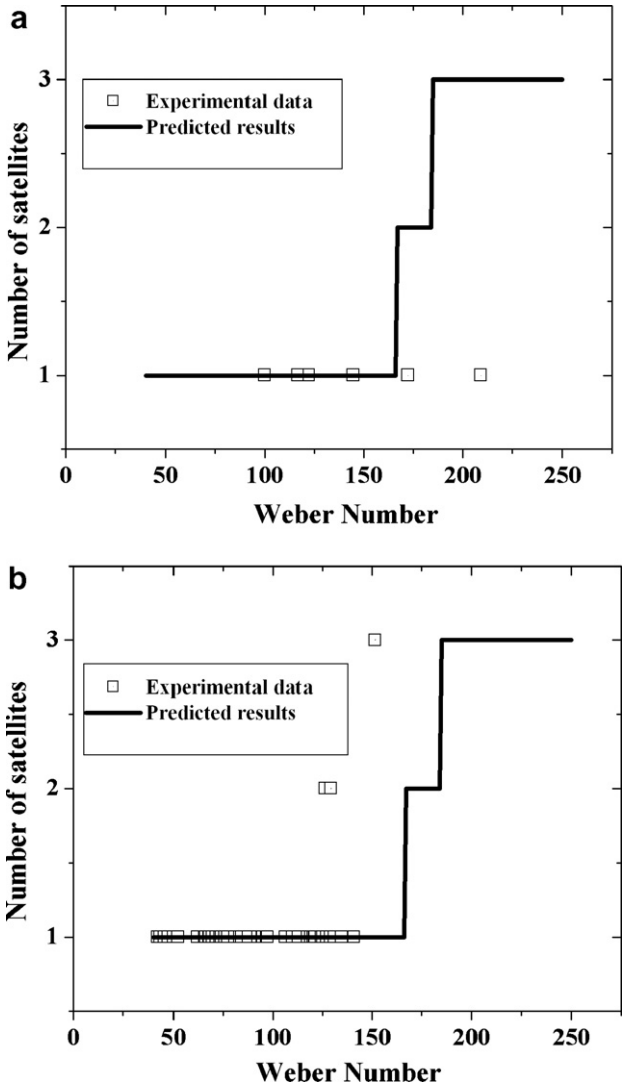

Fig. 11. Experimental and predicted number of satellite drops in reflexive separation (a) for colliding equal-size propanol-2 drops with drop diameter 110 μm (Brenn et al., 2001) (b) equal-size ethanol drops with drop diameter of 200 μm (Estrade et al., 1999).

experimental results of Brenn et al. (2001) are shown and the simulations over-predict the number of satellites at high Weber numbers. In Fig. 11b, experimental results of Estrade et al. (1999) are superimposed. The agreement is reasonable at lower Weber numbers but now the model under-predicts the number of satellites. The trend of an increase in the number of satellites as Weber number increases is captured.

4.4. Validation with data for colliding droplet streams

The present collision model was implemented into a modified version of the computational fluid dynamic code KIVA3V (Amsden, 1997) which solves for unsteady, compressible, reacting flows on finite volume grids. For the present laminar flow calculations, the mass and momentum conservation equations for the continuous fluid phase are

$$\frac{\partial \rho_f}{\partial t} + \nabla \cdot (\rho_f \bar{u}) = \dot{\rho}_f^s \tag{42}$$

and

$$\frac{\partial(\rho_f \bar{u})}{\partial t} + \nabla \cdot (\rho_f \bar{u}\bar{u}) = F^s - \nabla p + \nabla \cdot \sigma_L + \rho_f \bar{g}, \tag{43}$$

where ρ_f is the total fluid density, $\bar{u}$ is the fluid velocity, $\dot{\rho}_f^s$ is the spray source term, p is the fluid pressure, F^s is the rate of momentum gain per unit volume due to spray, $\bar{g}$ is the specific body force and σ_L is the laminar viscous stress tensor, which is Newtonian in form. In the standard code, the spray dynamics are solved using Monte Carlo methods and discrete particle (computational 'parcel') methods (Amsden et al., 1989). However, in the present study, the code was modified to track individual droplets so as to consider deterministic, trajectory based collision detections. The changes are summarized as follows:

(i) Each injected computational parcel contains one single drop.
(ii) Droplet drag and break-up processes were deactivated since only the collision process was of interest.
(iii) The collision impact parameter is determined from the geometry of the colliding drops (see Fig. 1). Further, if the sum of the droplet radii exceeds the distance between their centers leading to drop 'overlap', the probability of the collision is set to be unity. However, in the standard stochastic model (O'Rourke, 1981), neither the directions of movement of drops nor drop overlap is taken into account when deciding about the occurrence or non-occurrence of a collision.
(iv) Fragmentation is allowed to occur only if at least one satellite drop can be formed. Otherwise, the interacting drops simply undergo velocity changes reflecting energy and momentum conservation in both stretching (Eq. (2)) and reflexive separations (Eqs. (2) and (6)).
(v) In stretching separation, all satellite drops are put into a new parcel. In reflexive separation, two of the drops formed from the ligament break-up process are end-drops and the rest are put into a new parcel.
(vi) Collisions between two droplets formed from fragmentation are not allowed until the ligament break-up time for at least one of them is reached.

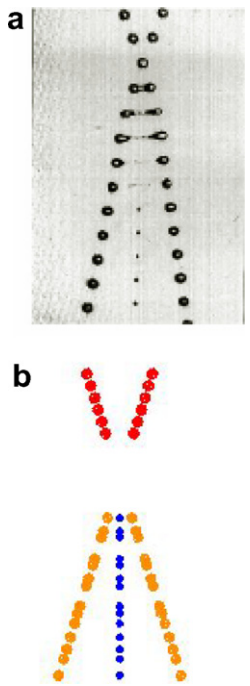

Fig. 12. Collision process for $We = 49$, $B = 0.57$, drop diameters = 105 μm. Droplets enter from top. (a) Experiments (Brenn et al., 2001) and (b) predictions.

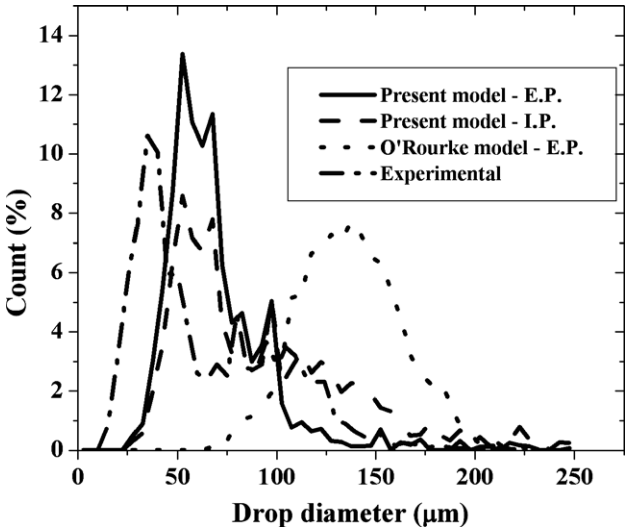

Fig. 13. Experimental (Hung, 1998) and predicted drop-size distributions for 10° collision angle. 'E.P.' denotes excluding parent drops and 'I.P.' denotes including the modified parent drops.

The present collision model was used to simulate results of Brenn et al. (2001) shown in Fig. 12a. Weber number is 49, impact parameter is 0.57 and the colliding drops are 105 μm in diameter. Fig. 12b is the corresponding simulation and the agreement is encouraging.

Hung (1998) studied colliding droplet streams of mineral spirits rule 66 (Stoddard solvent) produced by two sapphire plain-orifice nozzles. The arithmetic mean diameter (AMD) and velocity for the first stream of droplets were 131 μm and 23.21 m/s, respectively; for the second stream, the corresponding values were 138 μm and 16.4 m/s, respectively. The initial diameter distribution of injected droplets was nearly Gaussian.

In the experiments, single point measurements were made 2 cm directly below the point of collision. Since the colliding streams of poly-disperse drops travel at different velocities, there are uncertainties about the precise locations of the point of intersection. Accordingly, drop statistics were collected in two different ways to compare with the experimental data. In the first method, the statistics of parent drops were excluded. In the

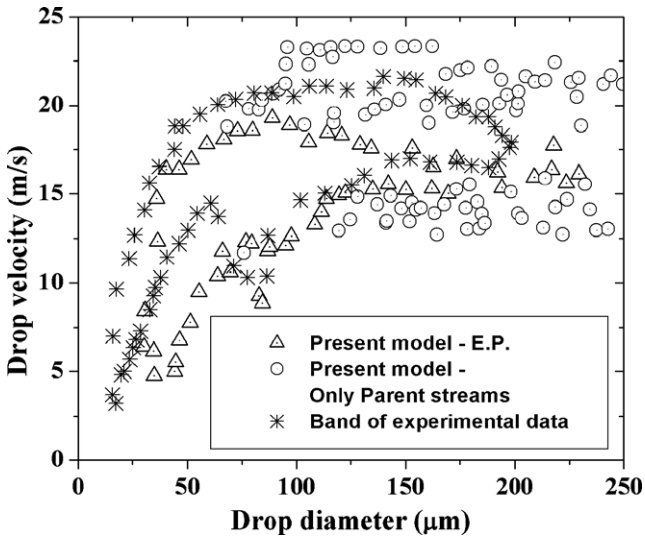

Fig. 14. Drop-size vs. velocity plots for 10° collision angle – predicted results along with the band of experimental results (Hung, 1998). 'E.P.' denotes excluding parent drops.

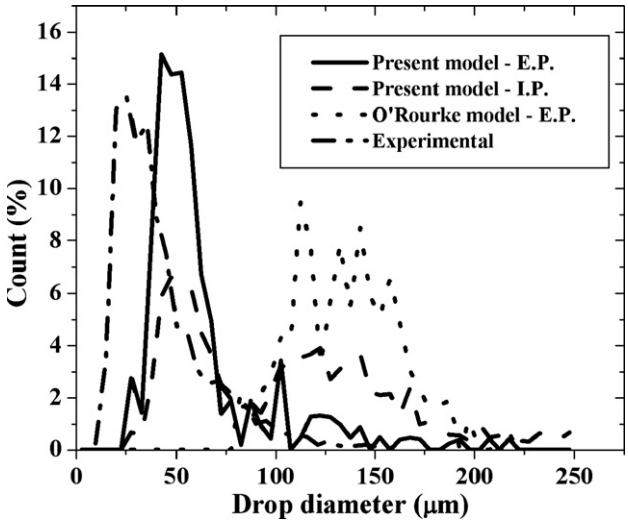

Fig. 15. Experimental (Hung, 1998) and predicted drop-size distributions for 20° collision angle. 'E.P.' denotes excluding parent drops and 'I.P.' denotes including the modified parent drops.

second method, as a limiting case, the modified (after collision) parent drops were also included in the statistics.

Fig. 13 compares the simulated post-collision drop-size distributions with the experimental data for collision angle of 10°. The experimental results show a bi-modal distribution with peaks at about 40 μm and 80 μm. The first peak predicted by the present model is at about 50 μm. However, inclusion of the modified parent drops in the statistics significantly changes the shape of the distribution. The experimental mean droplet diameter was 67.19 μm, while the present model predicts 73.18 μm when the modified parent drops are excluded and 99.17 μm when they are included. The overall agreement is considered to be good. Notice that the standard O'Rourke collision model highly over-predicts the drop-sizes, with a mean drop diameter 137.69 μm even when the modified parent drops are excluded, because it does not consider fragmentation.

Fig. 14 shows the range of the experimental drop-size–velocity correlation for the collision angle of 10° together with the corresponding predicted results. The ranges of drop velocities are seen to be nearly the same.

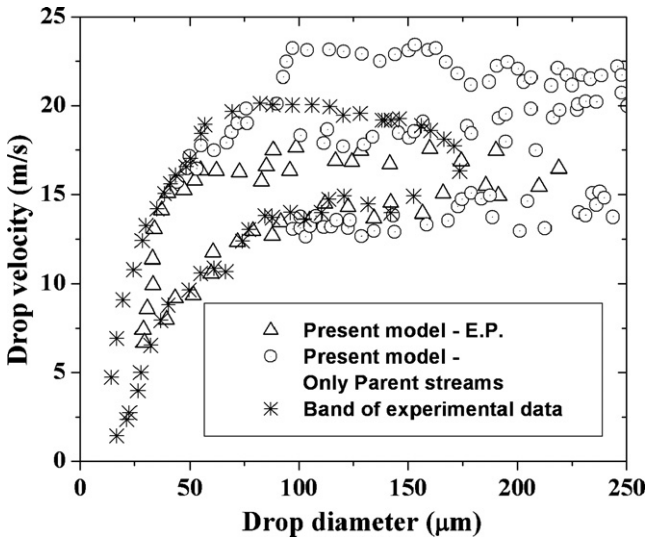

Fig. 16. Drop-size vs. velocity plots for 20° collision angle – predicted results along with the band of experimental results (Hung, 1998). 'E.P.' denotes excluding parent drops.

In both experimental measurements and predicted results, the droplets with diameter less than 100 μm have a proportional relationship between size and velocity and the dependency of the velocity on drop-size is weak at higher diameters.

Fig. 15 compares post-collision drop-size distributions for a collision angle of 20°. The experimental results show a uni-modal distribution with peak at about 25 μm while the predictions with parent drops excluded have the most probable diameter of about 40 μm. The mean droplet diameter observed in the experiments is 44.13 μm. The simulation results show a higher percentage of droplets between 100 μm and 150 μm, perhaps indicating some secondary coalescence process. Again, the O'Rourke model highly over-predicts the drop-sizes, with mean drop diameter being 135.32 μm when modified parent streams are excluded.

Fig. 16 shows the range of experimental drop-size–velocity data for the collision angle of 20° and the predictions. Again, the ranges of velocities agree with the experiments.

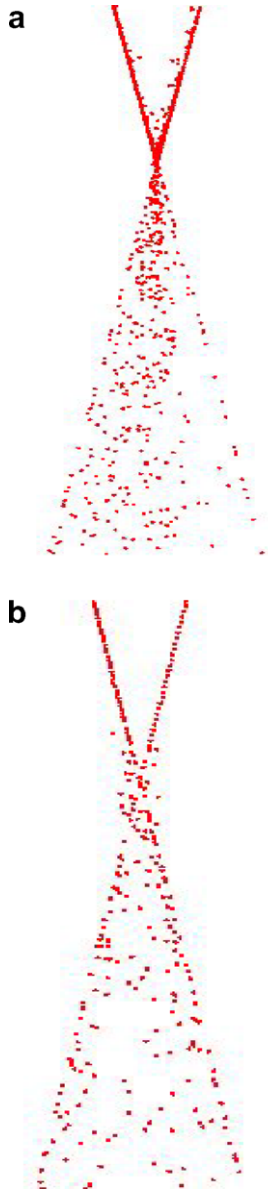

Fig. 17. Snapshots of the spatial droplet distribution close to the impingement point predicted for 20° collision angle: (a) present model and (b) O'Rourke model.

Fig. 17a shows a snapshot of the spatial droplet distribution close to the impingement point predicted by the present model, while Fig. 17b shows the corresponding snapshot from the O'Rourke collision model's results. The present model shows a 'core' formed by smaller size satellite drops due to the break-up of liquid ligaments while the O'Rourke model shows drops of relatively large diameter (see also Fig. 15) which are deflected from their original paths by the non-fragmenting collision process. The present model thus captures the physics of the fragmentation process more correctly.

Fig. 18 shows the total percentage count of each collision outcome for the collision angle of 10° as compared to the O'Rourke model. It shows that droplet bounce is an important process, but mainly coalescence and stretching separation compete with each other in determining the final drop distribution. Fig. 19 shows the corresponding results for the collision angle of 20°. The percentage of bounces is seen to be higher due to the increase in the collision angle.

Finally, Table 5 compares the CPU times required by the O'Rourke model and the present model for 10° and 20° collision angle cases. It can be seen that the additional computational expense introduced by the

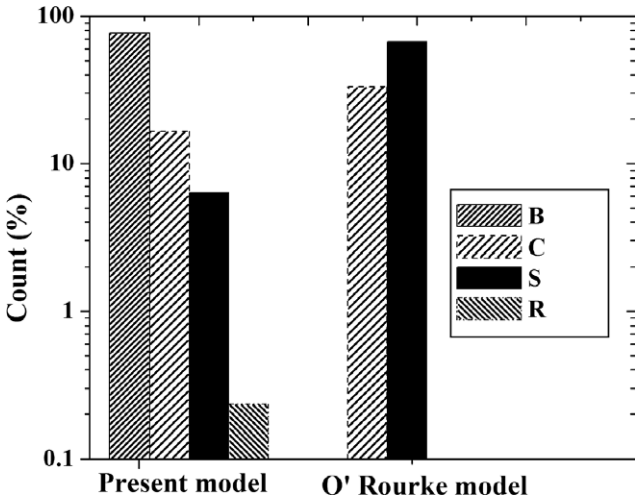

Fig. 18. Comparison of collision outcomes for 10° collision angle. 'B' – bounce, 'C' – coalescence, 'S' – stretching separation (present model)/grazing collision (O'Rourke model) and 'R' – reflexive separation.

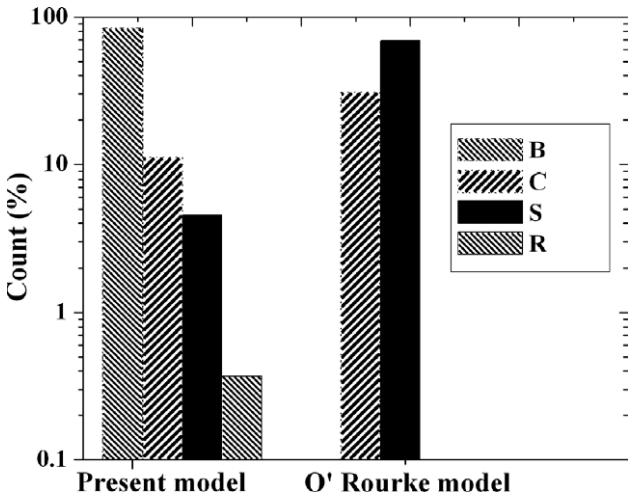

Fig. 19. Comparison of collision outcomes for 20° collision angle. 'B' – bounce, 'C' – coalescence, 'S' – stretching separation (present model)/grazing collision (O'Rourke model) and 'R' – reflexive separation.

Table 5
Comparison of CPU times for the two collision models

Collision angle (°)	CPU time – O'Rourke model (s)	CPU time – present model (s)
10	5020	5143
20	4804	5097

present model is modest. This is attributed to the predominance of bouncing which does not affect the number of drops, the avoidance of unphysical collisions, use of an approximate iterative solution method for ligament break-up and the additional expense of new drops created by fragmentation.

5. Conclusions

A new predictive model for binary drop collisions has been formulated that includes bouncing, coalescence, reflexive separation and stretching separation as outcomes. Comparisons with experimental data for tetradecane and ethanol drops colliding under atmospheric conditions show that the model predicts the collision outcomes reasonably well. Fragmentations in stretching and reflexive separations are modeled by assuming that the interacting droplets form an elongating ligament that either breaks up by capillary wave instability, or retracts to form a single satellite droplet. In stretching separation, the number of satellites formed is found to first increase with an increase in the impact parameter, reach a maximum and then decrease. The number of drops formed from fragmentation increases with an increase in Weber number. These trends are in agreement with experimental observations. The model was implemented into a CFD code and deterministic collisions were considered. Comparisons of model predictions with experiments for colliding poly-disperse drop streams were made. The results show that the present model predicts the outcome of the collision and relevant post-collision characteristics, such as drop-sizes, velocities and spatial distributions of droplets with acceptable accuracy and minimal added computational expenditure.

In the present model, drops formed from fragmentation are assumed to be uniform in size and velocity. Thus, the model does not predict the multiplicity of sizes observed in reality in a fragmentation process. An improved modeling approach could use a distribution function to define the characteristics of the droplets formed from ligament fragmentation. However, unequally sized drops have a greater tendency to coalesce and this process often competes with aerodynamic break-up even in a non-reactive spray to decide the final drop-size; so, considerations of such additional, competing processes should be important in spray applications.

Acknowledgements

The authors gratefully acknowledge the financial support provided by S.C. Johnson Wax through the Samuel C. Johnson Fellowship.

References

Amsden, A.A., 1997. KIVA-3V: a block structured KIVA program for engines with vertical or canted valves. Technical report No. LA-13313-MS, Los Alamos National Laboratory.

Amsden, A.A., O'Rourke, P.J., Butler, T.D., 1989. KIVA-II: a computer program for chemically reactive flows with sprays. Technical report No. LA-11560-MS, Los Alamos National Laboratory.

Ashgriz, N., Poo, J.Y., 1990. Coalescence and separation in binary collisions of liquid drops. J. Fluid Mech. 221, 183–204.

Brazier-Smith, P.R., Jennings, S.G., Latham, J., 1972. The interaction of falling rain drops: coalescence. Proc. R. Soc. London, Ser. A 326, 393–408.

Brenn, G., Valkovska, D., Danov, K.D., 2001. The formation of satellite droplets by unstable binary drop collisions. Phys. Fluids 13, 2463–2477.

Estrade, J.-P., Carentz, H., Lavergne, G., Biscos, Y., 1999. Experimental investigation of dynamic binary collision of ethanol droplets – a model for droplet coalescence and bouncing. Int. J. Heat Fluid Flow 20, 486–491.

Frankel, I., Weihs, D., 1985. Stability of a capillary jet with linearly increasing axial velocity (with application to shaped charges). J. Fluid Mech. 155, 289–307.

Gavaises, M., Theodorakakos, A., Bergeles, G., Brenn, G., 1996. Evaluation of the effect of droplet collisions on spray mixing. Proc. Inst. Mech. Eng. 210, 465–475.

Georjon, T.L., Reitz, R.D., 1999. A drop-shattering collision model for multidimensional spray computations. Atomization Sprays 9, 231–245.

Henderson, D., Segur, H., Smolka, L.B., Wadati, M., 2000. The motion of a falling liquid ligament. Phys. Fluids 12, 550–565.

Hung, C., 1998. Insights into droplet behavior within high pressure diesel sprays. Ph.D. Dissertation, Deparment of Mechanical Engineering, University of Wisconsin-Madison, Madison, WI.

Jiang, Y.J., Umemura, A., Law, C.K., 1992. An experimental investigation on the collision behavior of hydrocarbon droplets. J. Fluid Mech. 234, 171–190.

Ko, G.-H., Ryou, H.S., 2005. Modeling of droplet collision-induced breakup process. Int. J. Multiphase Flow 31, 723–738.

Kollár, L., Farzaneh, M., Karev, A.R., 2005. Modeling droplet collision and coalescence in an icing wind tunnel and the influence of these processes on droplet size distribution. Int. J. Multiphase Flow 31, 69–92.

Marmottant, P., Villermaux, E., 2004. Fragmentation of stretched liquid ligaments. Phys. Fluids 16, 2732–2741.

Morozumi, Y., Ishizuka, H., Fukai, J., 2005. Criterion between permanent coalescence and separation for head-on binary droplet collision. Atomization Sprays 15, 61–80.

Neitzel, G.P., Dell'Aversana, P., 2002. Noncoalescence and nonwetting behavior of liquids. Annu. Rev. Fluid Mech. 34, 267–289.

Orme, M., 1997. Experiments on droplet collisions, bounce, coalescence and disruption. Prog. Energy Combust. Sci. 23, 65–79.

O'Rourke, P.J., 1981. Collective drop effects in vaporizing liquid sprays. Ph.D. Dissertation, Dept. Mech. Aerospace Engg., Princeton University, Princeton, NJ.

Post, S.L., Abraham, J., 2002. Modeling the outcome of drop–drop collisions in diesel sprays. Int. J. Multiphase Flow 28, 997–1019.

Qian, J., Law, C.K., 1997. Regimes of coalescence and separation in droplet collision. J. Fluid Mech. 331, 59–80.

Reitz, R.D., Bracco, F.V., 1986. Mechanisms of breakup of round liquids jets. In: Cheremisinoff, N.P. (Ed.), . In: The Encyclopedia of Fluid Mechanics, vol. 3. Gulf Publishing Co., Texas, pp. 233–249.

Schmidt, D.P., Rutland, C.J., 2000. A new droplet collision algorithm. J. Comput. Phys. 164, 62–80.

Stone, H.A., 1994. Dynamics of drop deformation and breakup in viscous fluids. Annu. Rev. Fluid Mech. 26, 65–102.

Stone, H.A., Bentley, B.J., Leal, L.G., 1986. An experimental study of transient effects in the breakup of viscous drops. J. Fluid Mech. 173, 131–158.

Tennison, P.J., Georjon, T.L., Farrell, P.V., Reitz, R.D., 1998. An experimental and numerical study of sprays from a common rail injection system for use in an HSDI diesel engine. SAE Tech. paper 980810.

Willis, K., Orme, M., 2003. Binary drop collisions in a vacuum environment: an experimental investigation of the role of viscosity. Exp. Fluids 34, 28–41.